

Background Oriented Schlieren

Pascal Aeschi, Sebastian Lang, Xeno Meienberg

Experimental Methods for Engineers
ETH Zürich, D-MAVT, Group 14 - 13.12.2018

Abstract

With the growing evolution of numerical and digital imaging methods in the last few decades, Background Oriented Schlieren emerged as one of the simplest techniques in order to study density and temperature variations in flow fields as only a camera and a (preferably) random background is needed. The method analyses optical displacements respective to an undisturbed background generated by density variations in the area of interest. The distorted background represents an integral along the line of sight of the lateral refractive index gradient at each measurement point. In this experiment we used this method for two different setups: the Marangoni effect in paraffin oil and a high pressure air nozzle. As the refractive index is related to the temperature, the Marangoni images yielded a scalar temperature field. The pressurized air nozzle generates an under-expanded flow with so called shock diamonds, whose length was determined using BOS. The method proves to be fast and easily applicable.

1. Introduction

Introduced in the late 1990s the Background Oriented Schlieren (BOS) is a relatively new but very powerful imaging technique. It is a deviation of the original Schlieren technique which allows the experimenter to visualize temperature and density variations in fluids. While the original Schlieren is an optical method where no quantitative statement can be made about the final recording on film or camera, the digital nature of BOS enables the analysis of the obtained data.

Physical Background

Both methods rely on the basic principle of the density-dependance of the refractive index. The local speed of light in a medium highly depends on how dense it is: the rule of thumb is the higher the density the lower the local speed of light which in turn is inversely related to the refractive index. As a result of the varying density and consequently local speed of light, the beam changes its direction since it always takes the shortest path according to Fermat's principle. Looking at a background through a medium of varying density, for example the air over hot asphalt in the summer, one can observe that the background is distorted in comparison to a medium of constant density.

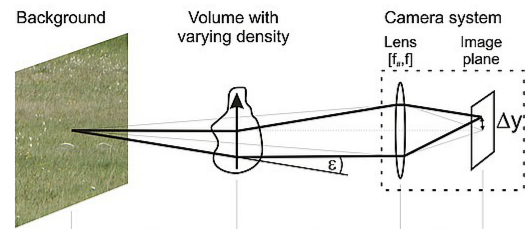


Figure 1: Light beam deflection due to density gradients measured by Schlieren method [www.dlr.de]

The measured (eye, image sensor) distorted wavefronts indicate a specific refractive index for every point on the displacement field in reference to the undistorted background. These refractive indices are related to the density through the Gladstone-Dale relationship:

2. Experimental Setup and Conditions

$$n - 1 = K\rho = K \frac{P}{RT} \quad (1)$$

where K is the Gladstone-Dale constant, which depends on the wavelength of the light used among other parameters.

Light Refraction

Considering a model, which describes the propagation of light through a medium with a varying refractive index there are two essential concepts: the wavefront and its respective propagating direction or ray.

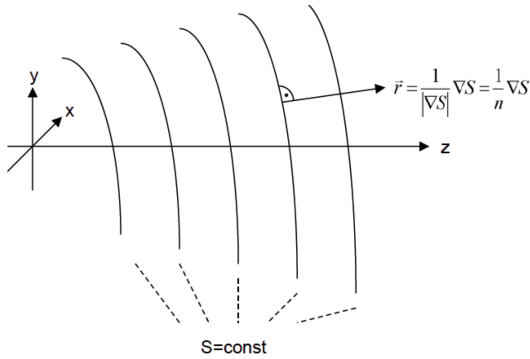


Figure 2: Wave fronts with $S = \text{const.}$ and rays \vec{r} [Handout BOS, v2.4]

where S denotes isolines of constant phase and the rays are vectors perpendicular to the wave fronts.

Derived from the Maxwell equations through simplifications emerges the Eikonal equation for path length S , which describes the propagation of waves.

$$\nabla S \cdot \nabla S = n^2(\vec{x}) \quad (2)$$

This equation can be solved using a perturbation (disturbance) approach:

$$n = n_0 + n_1(x, y, z); \quad n_1 \ll n_0 \quad (3)$$

$$S = n_0 z + S_1(x, y, z); \quad S_1 \ll n_0 z \quad (4)$$

where n_0 is the unperturbed refraction index and n_1 denotes the much smaller disturbance field. Using the definition of a ray as a normal vector on the phase surfaces and the solution integral for the disturbed phase $S_1(x, y, z) = \int_{z_0}^z n_1(x, y, z) dz$, the direction of the ray results in

$$\tan(\varepsilon_x) = \frac{r_x}{r_z} \approx \frac{1}{\frac{n_0}{n_0}} \frac{1}{n_0} \frac{\partial S_1}{\partial x} = \frac{1}{n_0} \int_{z_0}^z \frac{\partial n_1(x, y, z)}{\partial x} dz \quad (5)$$

$$\tan(\varepsilon_y) = \frac{r_y}{r_z} \approx \frac{1}{\frac{n_0}{n_0}} \frac{1}{n_0} \frac{\partial S_1}{\partial y} = \frac{1}{n_0} \int_{z_0}^z \frac{\partial n_1(x, y, z)}{\partial y} dz \quad (6)$$

Marangoni Flow in a Convection Cell

The first experiment is conducted on a rectangular test cell which is filled with mineral oil. In our experiments, the oil used is paraffin, yet other oils would also suffice in order to study the so called “Marangoni Effect”. The effect can be observed if one heats one edge of the test cell and places a cooling material on the other edge. This can be achieved by using an electric resistor as the heater and a good thermal conductor on the cooler edge, e.g. copper. Due to convection, the density of the fluid changes significantly on the hot side and buoyancy effects cause the hotter fluid to rise to the surface. The resulting surface tension gradient (i.e. less surface tension in hotter fluid) transitions into a flow, which is defined as the Marangoni Flow, illustrated in Fig. 3.

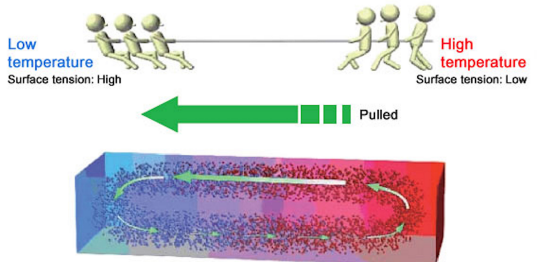


Figure 3: Marangoni Effect explained: Pulling resulting from surface tension gradients, [<http://iss.jaxa.jp/>]

As explained above, we try to extract the refractive indices by implementing a background of our test cell and then determine optical displacements of the background, which we compare to the original frame before neither convection nor displacements are present. In an ideal case under lab conditions, the background is chosen to be a random pattern, so that the later distorted image can be traced back to the original pattern. This can be achieved with similar algorithms which are used in PIV measurements. Instead of tracing particles, smaller subwindows of the pattern are generated. With discrete Fourier analysis, displacements of these subwindows can be computed. It should be noted that the displacements do not represent displacements of the fluid itself, they are induced by the resulting density gradients and therefore varying refractive indices. From experiments, it is known that the refractive indices of mineral oils and temperatures are linearly correlated

$$n(T) \approx 1.475 - 0.000374 \cdot (T - 20^\circ C) \quad (7)$$

It follows, that if we compute the refractive index distribution in the entire field, we can determine the temperature distribution simultaneously. If we had to study

other fluids such as water or ideal gases, other relationships would apply and pressures would also have to be accounted for.

Nozzle Flow

Another application of Schlieren method is the detection and the tracing of shock waves in compressible flows. In our experiment, we create these shock waves with an air pump which is connected to a convenient nozzle, which we model as a convergent-divergent one. This accelerates the flow and it is possible to reach speeds greater than the speed of sound ($Ma > 1$), which we will try to do in the experiment. This happens if the tank pressure is greater than the critical pressure. From theory, it is known that convergent-divergent nozzles can create so called ?shock diamonds? if one increases the pressure from a reservoir to such extent, that the exit conditions of the divergent part of the nozzle do not affect the flow anymore, which leads to an under-expanded flow at sufficiently high pressures. The length of the resulting shock diamonds can be determined by the Emden relation

$$\lambda = k \cdot d_{jet} \sqrt{\frac{p_0}{p_{amb}} - \frac{p^*}{p_{amb}}} \quad (8)$$

whereas the diameter and the critical pressure have to be determined. The diameter size is measured with a ruler and the critical pressure can be calculated under the condition $Ma = 1$:

$$\frac{p_0}{p_{amb}} = \left(1 + \frac{\gamma - 1}{2} \cdot Ma_{jet}^2\right)^{\frac{\gamma}{\gamma-1}} \quad (9)$$

Again, we use the background pattern as our reference and then compare observe the displacements due to density variations. We cannot exactly determine the resulting density variations, this comes from the fact that the region in which these diamonds occur is considerably small, thus strong gradients cannot give us results from a quantitative standpoint. One rather measures the positions where these high gradients occur. The Emden equation can be shown by measuring the distance between those diamonds, hence the unknown parameter k , which is known assumed to be 0.88 from empirical observations. Since this is a dimensionless parameter we can compare our measurements of multiple tank pressures against each other. *is determined empirically, we have to measure the distances at multiple pressures.*

3. Experimental Setup

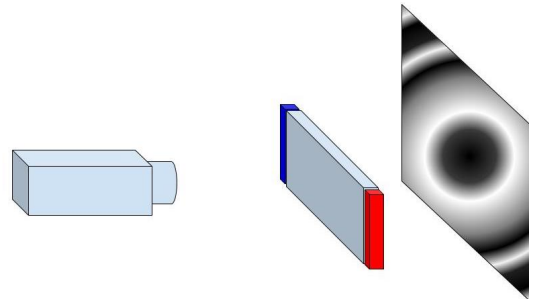


Figure 4: Symbolical Setup of the Marangoni Flow Experiment

The list of appliances needed to conduct the experiments is significantly modest. As mentioned, a pattern is used in the background. Additionally, a camera can be mounted on a rail, while for the first phase of the experiment, the flow cell is mounted on the rail as well such that all objects are ideally aligned. The camera is triggered externally by a computer and sends the raw pictures back in result (Fig. 4). It is of importance, that the background and cell remain in focus in order to process the data correctly. The temperature for the heat sink is assumed to be the measured room temperature, because copper has a very high thermal conductivity and thus is quick to adapt to thermal equilibrium with the surroundings. The temperature of the heater is measured by placing a liquid crystal indicator strip.

In the second phase of the experiments, the nozzle used for the Emden parameter evaluation is placed such that the flow is perpendicular to the image plane. The nozzle is mounted on a vessel whose pressure we calibrate continuously by hand. The vessel has to be connected to a source of air. Often, the valves connected to gas sources have integrated pressure sensors or barometers, yet one has to install an additional barometer at the exit of the valve (Fig. 5). This comes from the fact that pressure losses from the source to the exit also have to be included, thus errors are minimized by measuring the pressure at the valve once more. In addition, one always has to check the barometer scalings and parameters accurately. In our setup, pressure measurements are made relative to ambient pressure, whereas other barometers may display total pressures. Accordingly, the ambient pressure has to be determined as well.

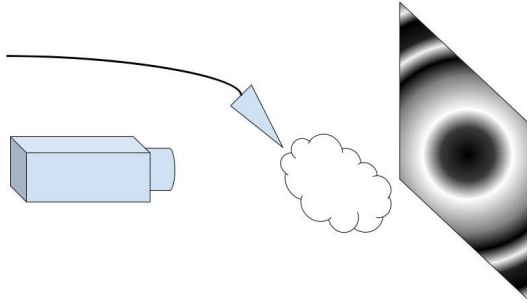


Figure 5: Symbolical Setup of the Nozzle Flow Experiment

Measurements and Results

Marangoni Cell

The obtained refractive index distribution and consequently the temperature distributions after five minutes and ten minutes are given below in Fig. 6, 7, 8 and 9. From the theory given, we know that the refractive indices are represented by isolines of the wavefronts, which were integrated numerically in Matlab by a polynomial of the order of 5 additionally to the already calculated refractive indices from the temperature at each edge. Evidently, the refractive index varies between those edges. Since the scales of the differences of the refractive indices are in a range between 1.4693 and 1.4744 at the hot and the cold edge respectively, the scaling of the iso-surfaces was chosen to be about 0.0001 increments, what resulted into 50 scaling steps. One can see that the refractive index in general decreases from left to right. It can be observed that the iso-surfaces of the refractive indices, especially in the middle of the section, are skewed. At the top, they tend towards the left edge while at the bottom of the cell they rather tend towards the right side. As soon as we move to the edges, we can see that the refractive indices along each surface is constant and in the bottom left corner and the upper right corner, a comparably larger area shows signs of a concentration. If one compares the two different time instances to each other, it can be observed that the skewness in the middle of the cross section is skewed a little bit more, especially at the bottom of the cross section. It seems that the indices are shifted from left to right at the bottom and slightly from right to left at the top.

The temperature profile shows the same profile qualitatively, the only difference between the temperature plots and the refractive index distributions is that that the temperatures follow the negative linear relation to the refractive index (Eq. 7) hence the colormap is inverted.

Nozzle Flow

From knowing the tank pressure as well as the ambient pressure we can calculate the Mach number. this can be

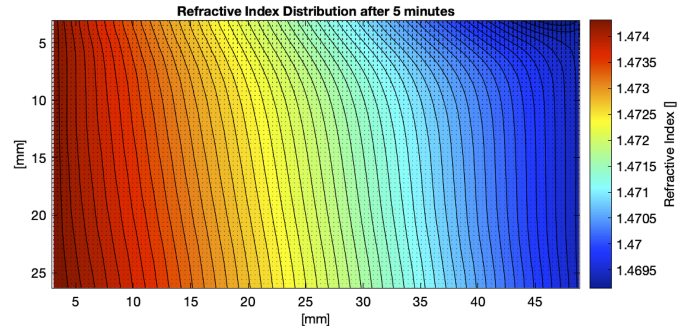


Figure 6: Refractive Index Distribution of the Marangoni Flow Experiment after 5 minutes runtime

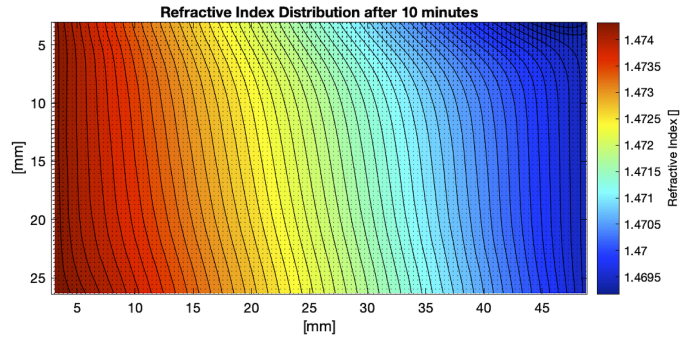


Figure 7: Refractive Index Distribution of the Marangoni Flow Experiment after 10 minutes runtime

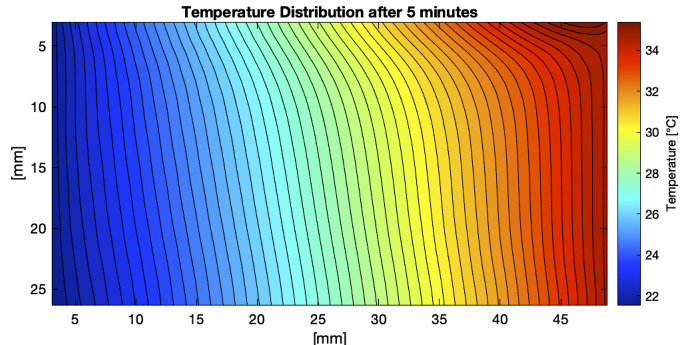


Figure 8: Temperature Distribution of the Marangoni Flow Experiment after 5 minutes runtime

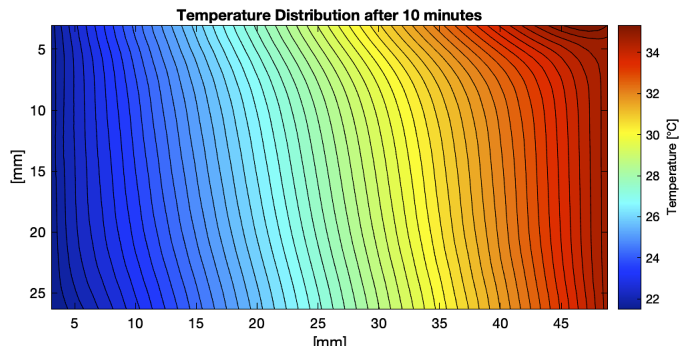


Figure 9: Temperature Distribution of the Marangoni Flow Experiment after 10 minutes runtime

seen in (Fig. 10) where it is plotted against rising tank pressure and a somewhat logarithmic curve can be observed. We obtain a Mach number of 1.3578 for a tank pressure of 3 bar ranging up to 1.9283 at 7 bar tank pressure.

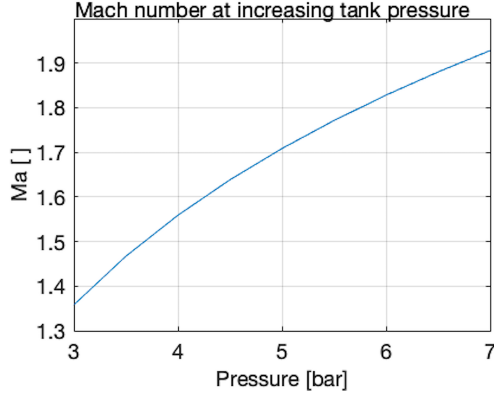


Figure 10

Measuring the wavelength of the pulses we receive a lambda of 3.8 mm for a tank pressure of 3 bar . This results in a k of 0.6019 which is close to the known value of 0.88 . There is still a deviation which might stem from different factors. First, the nozzle will have friction and thus be not isenthalpic which we did not consider. Also the camera resolution is not very exact at the scales we would need. Thus there is a measurement error there, but it is also hard to reliably and precisely measure the lambda from there. Also the measurement of the nozzle diameter has a very big uncertainty which strongly translates further. For example if the diameter was 5.5 mm we would already have $k = 0.6566$. Measuring with a ruler and the eye is not much more precise than 0.5 mm which on its own introduces a big error. Thus a multitude of factors influence the result and lead to the difference from the known value.

In Fig 11-14 we compare the displacement of the sonic booms with increasing tank pressure and thus Mach number. In the displacement map we see in Figure 11 compared to Figure 13 much smaller displacement bubbles which are closer together and more frequent. In Figure 14 we see larger bubbles that are still comparatively large even after losing almost all of their intensity. There we also can observe the increase in lambda with increasing tank pressure. In the Pseudo Schlieren image at 3 bar (Fig. 12) we have a zone of very limited activity directly before the shock, while in Fig 14 there is activity there even though it is decreased compared to the other areas. After that shock we can observe strong activity that split in an upper stream and a lower stream which are almost symmetric. We also observe strong intensity directly after

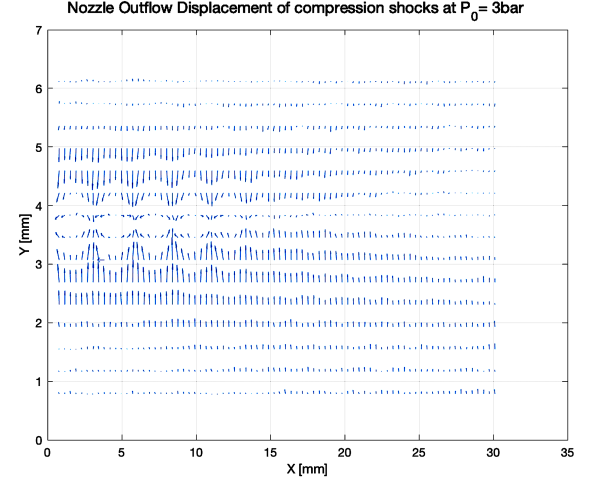


Figure 11

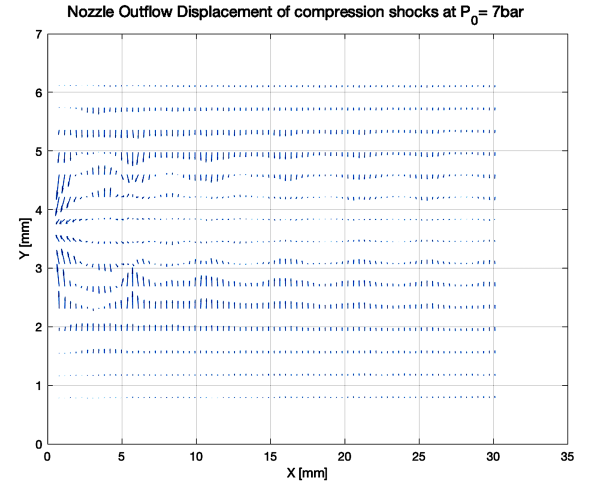


Figure 12

the nozzle. The intensity is much stronger at higher tank pressure and the gradient within the image is as well.

4. Discussion and Conclusion

Marangoni Cell

All in all, we could observe a very well distributed temperature, whereas the quality of the whole distribution did not change significantly over the whole cross section. The edges, especially the top right, “hot” corner and the bottom left, “cold” corner were displaying some kind of concentration, area of hot or cold fluid. This might come from the fact that since the less dense fluid rises to the top, it rather does not change its density rapidly. The velocity is rather small and the surface tension gradient is small as well since we do not have large temperature gradients, assuming the temperature difference of both edges is around

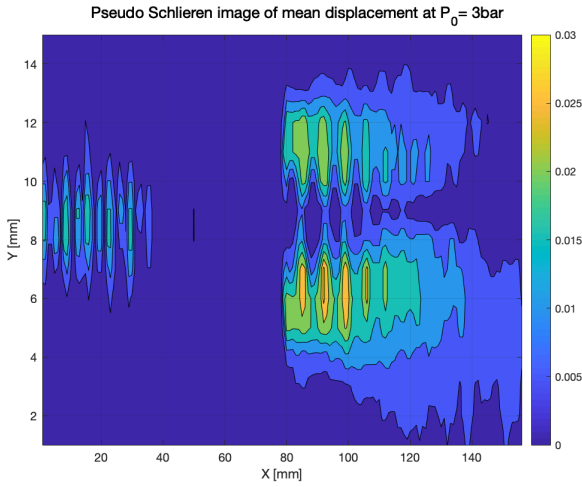


Figure 13

13.5 *K*. Qualitatively, the pull effect of the surface tension can still be seen, yet it does not appear to be of high magnitude. This tells us the Marangoni effect is present. We can see that the runtime of ten minutes compared to five minutes does not change the temperature distribution really much, it seems that the “Schlieren” does not distort the images taken as much as expected. If we had measured the effect in larger timescales, we might have seen more change in the overall profile. In our model, we considered the edges to have constant temperature. Interestingly enough, we could see that if the index gradients of the whole field are determined and later on transformed back into temperatures, that they do not show any uniformity at each of the edges. Our model equation proposed in (Eq. 7) for the refractive index does not alter the temperature profile qualitatively. If we include deficiencies in the materials used (the copper block, convection from the glass, other losses), we may be able to extend the model further, hence better temperature distributions may be found from a quantitative standpoint. For further analysis one could consider using a poisson solver and compare the obtained data with those we obtained above. In total, with the basic setup which we have used, we could still fetch acceptable results from simple images and optically, temperature distributions as well as the Marangoni Flow could be studied in a reasonable range.

Nozzle Flow

We observed a k which varied a bit which is mostly due to measurement inaccuracies but also were consistently $\approx 20\%$ off. This is possible to stem from the fact that the nozzle is not characterized correctly. The diameter was only measured with an inaccurate tool. Also the assumption for the nozzle to be isentropic is not true, as there is friction taking place which we do not account for. This could be improved with more exact knowledge about the nozzle to develop a more accurate model. The resolution of the supersonic cells is also a point which could drastically be improved, as these cells are quite small especially for lower tank pressures. But this would require a much better camera, which is a lot more expensive, as well as increasing the amount of data points generated and with that the computational effort required. The abrupt jump after the shock in the pseudo schlieren image could maybe be evaluated by for example acoustic measurements to get more insight in the irreversibility of the sonic boom. In conclusion, we observed the supersonic cell characteristic of an under-expanded jet and measured the impact of increasing tank pressure which leads to bigger more spaced out shock cells.

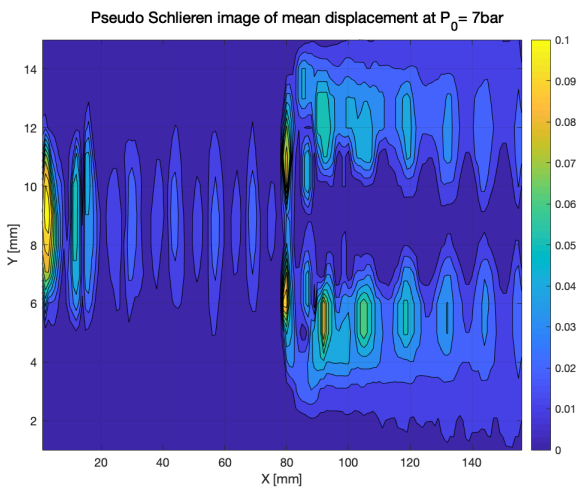


Figure 14